http://dx.doi.org/10.1595/205651315X689117 Johnson Matthey Technol. Rev., 2015, 59, (4), 303–312

JOHNSON MATTHEY
TECHNOLOGY REVIEW
www.technology.matthey.com

Interplay between Silver and Gold Nanoparticles in Production of Hydrogen from Methanol

Developing a highly stable bimetallic catalyst for fuel cell applications

By Hany M. AbdelDayem
Chemistry Department, Faculty of Science, Ain Shams University, 11566 Abbassia, Cairo, Egypt

Email: hany.mohammed@sci.asu.edu.eg; monamohus@yahoo.com

Hydrogen production from methanol oxidation over silver-gold/zinc oxide (AgAu/ZnO) catalysts was investigated. Bimetallic catalysts produced higher hydrogen yield and lower carbon monoxide and water yields than Ag/ZnO catalyst without deactivation during 72 h on stream at 250ºC. In addition, the presence of Au in the bimetallic catalyst facilitated the preferential oxidation of CO to CO_2. Structural analysis of bimetallic catalysts indicated that the strong interaction between Ag and Au particles in the nano-range (4.2 nm–7.2 nm) efficiently enhanced the reducibility of non-selective silver oxide (Ag_2O) species. Furthermore dispersion of metal particles in bimetallic AgAu/ZnO catalysts did not significantly change after reaction; however, dispersion of Ag species in Ag/ZnO catalyst was remarkably decreased.

1. Introduction

Direct partial oxidation of methanol (POM) to hydrogen reduces the complexity of hydrogen-fuelled proton exchange membrane (PEM) fuel cells. Methanol can be easily oxidised into hydrogen at relatively low temperatures (<250ºC) (1, 2). In addition, it contains no carbon-carbon bond and it has a high H:C ratio therefore reducing the risk of coke formation and catalyst fouling.

Bimetallic catalysts based on noble metals (gold, silver and platinum) and copper are known to be more active for hydrogen production from methanol than monometallic ones (3–18). Ag has the lowest price among noble metals, which makes it ideal for use as an industrial oxidation catalyst. The electrochemical and steam reforming activity of bimetallic catalysts based on Ag has been studied extensively (18–22). However, there are few studies in the literature dealing with direct POM to hydrogen on Ag-based catalysts (9, 23–25). Recently, Ag/ZnO catalyst was found to be active for POM to hydrogen; however, the catalyst produced high CO yield (~6%) and was rapidly deactivated (25). On the other hand, bimetallic combinations such as Au-Ag significantly improved the activity and the stability of Ag catalyst in CO oxidation to CO_2 at low temperature (26–32). Furthermore, much attention has been focused on using Ag-Au bimetallic catalysts for other important reactions such as oxidation of alcohols, dechlorination of organochlorides, hydrocarbon-selective catalytic reduction of nitrogen oxides (NOx), decomposition of organic pollutants, hydrogenation of esters and ethylene oxidation (33–40). The activity in a desired application is determined by the oxidation state of the reactive species, interaction between Ag and Au particles, the particle size, shape and location on the support controlled by the preparation process and the nature of the support (41, 42).

The main objective of this work was to develop a highly stable bimetallic catalyst based on noble metals (Ag and Au) with high performance in the oxidation

of methanol to hydrogen with low CO formation. The effect of adding Au on the physicochemical properties of Ag/ZnO was also studied.

2. Experimental

2.1 Catalysts Preparation

2.1.1 Preparation of Zinc Oxide Support

Nano-sized ZnO support was synthesised by direct precipitation (25). Analytical grade zinc nitrate ($Zn(NO_3)_2$) and ammonium carbonate ($(NH_4)_2CO_3$) (Sigma-Aldrich, 99.5%) were first dissolved in deionised water to form solutions of 1.5 mol l^{-1} and 2.25 mol l^{-1}, respectively. The $Zn(NO_3)_2$ solution was slowly poured into the $(NH_4)_2CO_3$ solution with vigorous stirring and then the precipitate derived from the reaction was collected by filtration and rinsed three times with high-purity water and ethanol. The product was dried at 80ºC to form the ZnO precursor. Finally, the precursor was calcined at 550ºC for 2 h in a muffle furnace to obtain nanoscale ZnO particles. The average crystal size of ZnO was *ca.* 35.2 nm, calculated from X-ray diffraction (XRD) by the Debye-Scherrer formula (25).

2.1.2 Preparation of Monometallic (Silver or Gold) Catalysts

The preparation of either Au/ZnO_2 or Ag/ZnO_2 catalyst with 5.0 wt% as theoretical loading was performed by deposition-precipitation (DP) with sodium carbonate (Na_2CO_3) at pH 8.5. Gold(III) chloride trihydrate ($HAuCl_4 \cdot 3H_2O$) and silver nitrate ($AgNO_3$), both from Sigma-Aldrich, were used as Au and Ag precursors. ZnO support was suspended in an aqueous solution of metal precursor, then the pH was controlled by the addition of 0.5 M Na_2CO_3. After DP, all samples were centrifuged, washed with water four times, centrifuged again and dried under vacuum for 2 h at 80ºC. After drying, the samples were stored at room temperature in desiccators under vacuum, away from light, in order to prevent any alteration (26, 43). Catalysts were calcined at 300ºC for 3 h.

2.1.3 Preparation of Bimetallic Catalysts

Preparation of bimetallic $Ag_{1-y}Au_y$ (y = 0.1, 0.25 and 0.5, where y is the mass fraction of Au with respect to sum of weights of Au and Ag) catalysts supported on ZnO with 5.0 wt% as theoretical loading were also performed by DP with Na_2CO_3. The oxide support was suspended in an aqueous solution of $HAuCl_4 \cdot 3H_2O$ and $AgNO_3$. The initial pH was ~3, which was then adjusted to 8.5 by drop wise addition of 0.5 M Na_2CO_3 to promote metal hydroxide precipitation on zinc peroxide (ZnO_2). The obtained samples were washed, dried, stored and calcined as described above.

2.1.4 Preparation of Silver and Gold Mechanical Mixture

The mechanical mixture $(Ag_{0.5}Au_{0.5}Zn)_{mix}$ catalyst was prepared by dispersing equal amounts of both 2.5 wt% Ag/ZnO and 2.5 wt% Au/ZnO powders (prepared by DP) in 200 ml *n*-pentane to give a total of 5 wt% metals as theoretical loading. The suspension was stirred vigorously for 20 min and then ultrasonically for 5 min. The *n*-pentane was evaporated at 40ºC and the obtained solid was dried at 100ºC overnight without further calcination.

2.2 Catalysts Characterisation

The Ag and Au content in these catalysts was determined by atomic absorption spectroscopy (AAS) on a Perkin Elmer model 3100. XRD measurements were performed on a Philips X'Pert multipurpose X-ray diffractometer (MPD) using Cu $K_{\alpha1,2}$ radiation (λ = 1.5405 Å) for 2θ angles varying from 10º to 80º. Hydrogen temperature-programmed reduction (H_2-TPR) was performed using a ChemBET 300 Quantachrome. 100 mg sample of the freshly calcined catalyst was subjected to a heat treatment (20ºC min^{-1} up to 1000ºC) in a gas flow (85 ml min^{-1}) composed of a mixture of 5 vol% hydrogen and 95 vol% nitrogen. Prior to the TPR experiments, the samples were heated for 3 h under an inert atmosphere (nitrogen) at 200ºC. The surface areas (S_{BET}) of the various samples were determined from the adsorption of nitrogen gas at liquid nitrogen temperature (–195.8ºC) using a NOVA3200e (Quantachrome Instruments, USA). Before the measurements, all samples were perfectly degassed at 150ºC and 10^{-4} Torr overnight. Transmission electron micrographs were obtained using a JEOL 1200 EX II transmission electron microscope (TEM) operated with an acceleration voltage of 50 kV. Nitrous oxide (N_2O) pulse chemisorption was applied to determine the Ag degree of dispersion using ChemBET 3000 and the TPR-Win V. 1.50 software; further details can be found elsewhere (25). Energy dispersive X-ray analyses (EDX) were recorded using a Quanta FEG 250 microscope, equipped with EDX spectrometer (TexSEM Laboratories (TSL) EDAX, AMETEK, Inc, USA). Ultraviolet-visible (UV-Vis) reflection spectra were recorded on a JASCO V-570 spectrophotometer.

2.3 Catalytic Test

Catalytic tests were performed at atmospheric pressure in a tubular quartz reactor with 6 mm internal diameter. The reaction was carried out at 250ºC and in a differential mode at conversion *ca.* 5% by varying the space velocity through changing the catalyst weight. The feed and product gas compositions were determined by online gas chromatography (GC), using a Bruker 450 GC equipped with three channels. The first is for hydrogen analysis using a thermal conductivity detector (TCD). The gas separation was performed by HayeSep Q and 5 Å molecular sieves. Channel two is for analysing non-flammable gases (O_2, N_2, CO and CO_2) using TCD and separation was accomplished by HayeSep Q and MolSieve 13X columns connected in series. The third channel is for analysing oxygenates (methanol, formic acid and formaldehyde) and separation was accomplished by HayeSep Q and Varian Select™ columns. The catalyst was diluted with silicon dioxide (SiO_2) to 10 wt% to prevent hot-spot formation in the bed. The catalyst activation was performed *in situ* by exposing the catalyst to 100 ml min^{-1} of 10% H_2/N_2 and increasing the temperature to 250ºC at 10ºC min^{-1}. This temperature was maintained for 1 h. Subsequently, the furnace temperature was lowered to ~100ºC. The partial oxidation experiments were performed under a total flow rate of 220 ml min^{-1} with an O_2/methanol molar ratio of 0.5, balanced with nitrogen and the weight hourly space velocity (WHSV) was from 8.8 × 10^4 ml h^{-1} g^{-1} to 13.2 × 10^4 ml h^{-1} g^{-1} (WHSV = flow rate of feed gas (ml h^{-1}) per weight of catalyst (g)). The catalysts' stability was examined followed by the change of the rate of hydrogen production at a higher temperature i.e. 350ºC and at iso-conversion 5% by changing WHSV from 14.7 × 10^4 ml h^{-1} g^{-1} to 18.9 ×10^4 ml h^{-1} g^{-1}. Furthermore, the external and internal mass transfer limitations of the catalytic system were tested. Catalytic tests were carried out using different particle sizes of AgZn and $Ag_{0.5}Au_{0.5}Zn$ catalysts in the range 125 µm–1000 µm at the constant WHSV = 8.8 × 10^4 ml h^{-1} g^{-1} and 13.2 × 10^4 ml h^{-1} g^{-1}, respectively. The results showed that catalyst of particle sizes 212 µm to 710 µm exhibited constant conversion without pressure drop at the constant WHSV. Thus the catalysts were ground and sieved to 355 µm−500 µm. In addition, the calculation of effectiveness factor (η) for AgZn sample with an average particle diameter of 356 µm showed that the values are close to 1.0; at iso-conversion 5%, T = 350ºC and WHSV = 8.8 × 10^4 ml h^{-1} g^{-1}, indicating no internal diffusion limitation in the catalytic system. The activity of the catalyst was expressed in terms of experimental rate ($Rate_{expt}$ = mmole of products per gram catalyst). The following formula (Equation (i)) was used to calculate the theoretical rate ($Rate_{theort}$) of hydrogen production over AgAuZn catalysts:

$$Rate_{theort} = Rate_{expt} \text{ of AgZn } (1–y) + Rate_{expt} \text{ of AuZn } (y) \quad \text{(i)}$$

3. Results and Discussion

In the case of bimetallic samples, the actual Ag and Au fractions are also very close to the nominal values (**Table I**). **Table I** shows the measured values of the

Table I Characterisation of the Catalysts

Catalyst	Nominal fraction	Ag, %[a]	Au, %[a]	Actual fraction	S_{BET}, m^2 g^{-1}[b]	Metal dispersion[c], %	XRD crystal size[f]
ZnO	–	–	–	–	38.8	–	
AgZn	–	4.6	0	–	36.3	42.0 (28.1)[e]	5.8
AuZn	–	0	4.5	–	36.9	46.9 (32.0)	4.2
$Ag_{0.9}Au_{0.1}Zn$	0.1	4.3	0.4	0.09	36.4	41.5 (37.3)	6.1
$Ag_{0.75}Au_{0.25}Zn$	0.25	3.5	1.1	0.24	35.7	39.8 (38.2)	6.4
$Ag_{0.5}Au_{0.5}Zn$	0.5	2.3	2.2	0.49	37.0	38.3 (37.1)	7.2

[a] Weight percentage from atomic absorption spectroscopy
[b] From N_2 adsorption
[c] Ag and/or Au
[e] Value in parenthesis is metal dispersion after reaction
[f] Calculated from XRD peak at 2θ ~38.1º

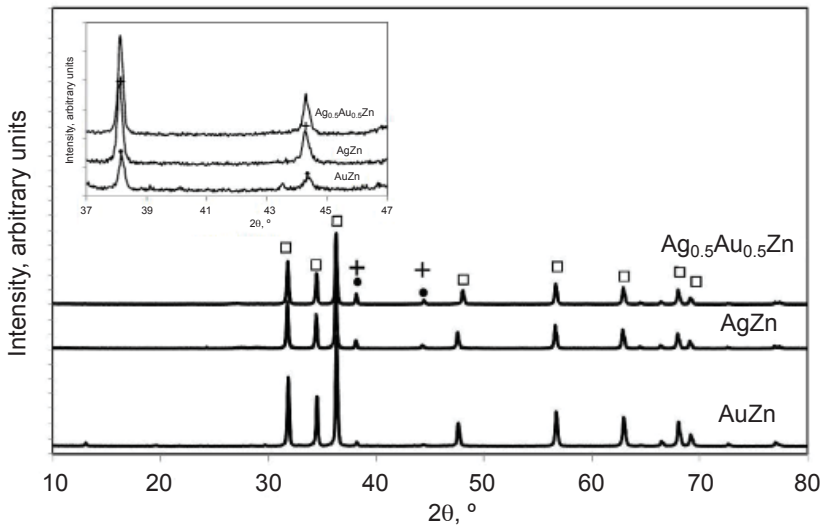

Fig. 1. Wide-angle XRD patterns of the AgZn, AuZn and $Ag_{0.5}Au_{0.5}Zn$ catalysts. Figure inset XRD patterns of the same catalysts in the range 37° to 47°. Peaks marked by the symbols "□", "+" and "●" indicate the peaks assigned to ZnO, Ag_2O and metallic Au, respectively

BET surface areas of catalysts. Interestingly, the BET surface area of the ZnO support was not significantly altered after loading of Ag or Au or both. The results of N_2O chemisorptions shows that the degree of dispersion of Ag in Au-containing catalysts (i.e. bimetallic samples) was less than in AgZn by *ca.* 4% (shown in **Table I**). This may suggest an interaction between Ag and Au particles in the bimetallic catalysts. The lower dispersion of Ag and Au particles on ZnO in bimetallic catalysts was clearly verified by an increase of crystallite size of metals measured by XRD (**Table I**).

Figure 1 shows XRD patterns of AgZn, AuZn and $Ag_{0.5}Au_{0.5}Zn$ catalysts. All of the diffraction peaks of ZnO could be indexed to the hexagonal phase reported in the Joint Committee on Powder Diffraction Standards (JCPDS) file (36-1451). For AgZn catalyst, the peaks characteristic of the cubic Ag_2O phase were detected at 2θ = 38.08° and 44.29° (JCPDS file, 65-3289 and 42-0874). In the case of AuZn catalyst the peaks at 2θ = 38.17° and 44.38° are characteristic of the single pure metallic Au phase (JCPDS 04-0784). However, in the case of $Ag_{0.5}Au_{0.5}Zn$ catalysts, Au-Ag alloy could not be distinguished from Ag_2O and metallic Au based on the XRD patterns because the diffraction lines characteristic of Au and Ag are overlapped.

Based on both XRD and TEM results, both Ag particles and Au particles supported on ZnO in monometallic and bimetallic catalysts were in the nano-range 4.2 nm–7.2 nm (see **Table I** and **Figure 2**). The average size of the Ag particles in the bimetallic $Ag_{0.5}Au_{0.5}Zn$ catalyst (**Figure 2(b)**) was larger than that in the monometallic AgZn catalyst (**Figure 2(a)**). Furthermore, as shown from the TEM micrograph of $(Ag_{0.5}Au_{0.5}Zn)_{mix}$, the contact between Ag and Au particles was lower than that between these particles in $Ag_{0.5}Au_{0.5}Zn$ (**Figure 2(c)**). This suggests that Ag-Au ensembles may be formed due to the interaction between Ag and Au. On the other hand, the elemental ratio of Au:Ag by EDX for $Ag_{0.5}Au_{0.5}Zn$ catalyst was 0.86 as shown in the EDX pattern (**Figure 3(a)**), i.e. the Ag-Au composite composition was approaching 1:1. However, the Au-Ag ratio for the same catalyst prepared by mechanical

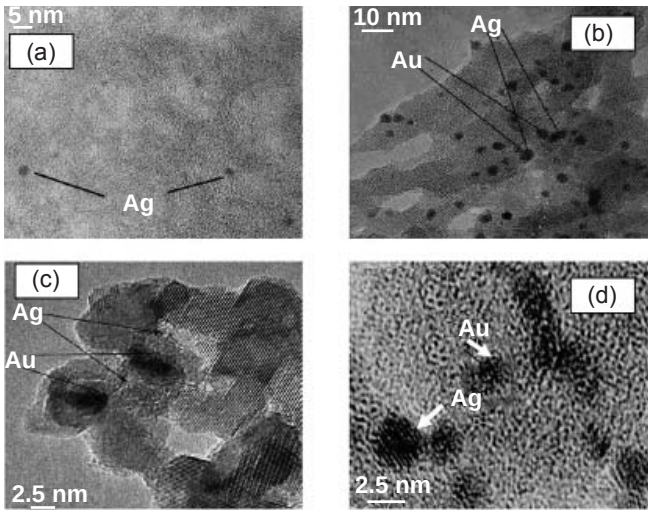

Fig. 2. TEM micrographs of the catalysts: (a) AgZn; (b) and (c) $Ag_{0.5}Au_{0.5}Zn$ prepared by DP method at different magnifications from ×100,000 to ×350,000 and (d) $(Ag_{0.5}Au_{0.5}Zn)_{mix}$ prepared by mechanical mixing

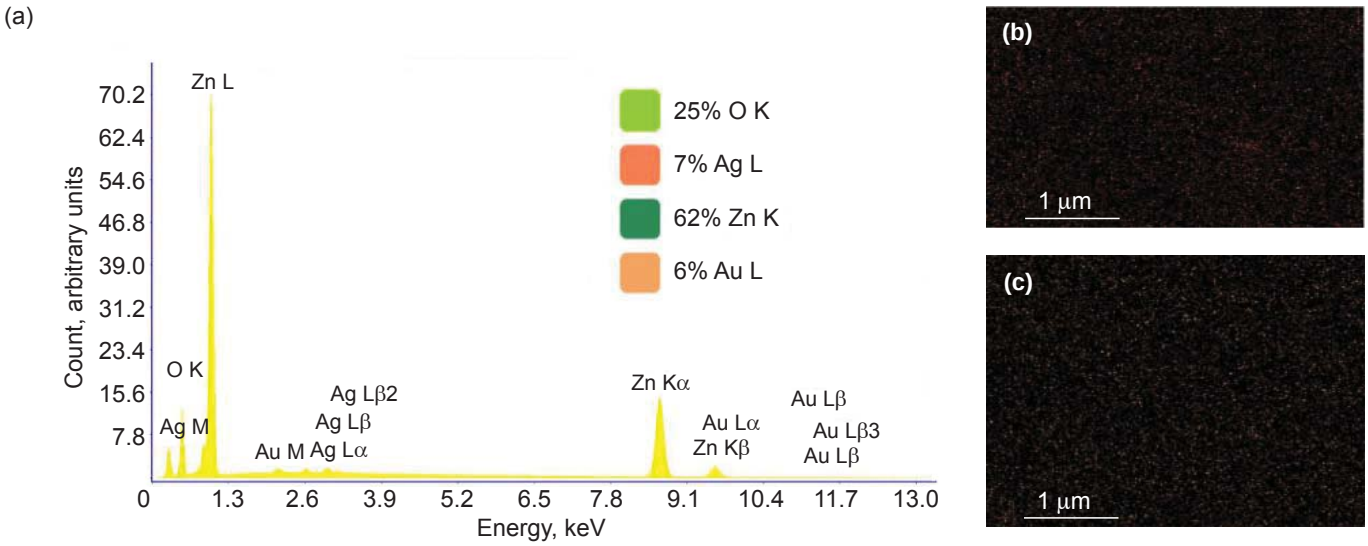

Fig. 3. $Ag_{0.5}Au_{0.5}Zn$: (a) EDX spectrum; (b) EDX mapping for Ag element: the region of mapping corresponds to (a), acquisition time 665.4 s; (c) EDX mapping for Au element; acquisition time 655.4 s

mixing was found to be 1.4, as estimated from the EDX pattern (**Figure 4(a)**). It was evident that the outer layers of the bimetallic mixture in this case is enriched in Au. From EDX mapping of the $Ag_{0.5}Au_{0.5}Zn$ catalyst (**Figures 3(b)** and **3(c)**), the contrast between Ag and Au was fairly clear in the homogeneous distribution occupying the same location on the ZnO top surface i.e. in good contact (44). However the EDX mapping of the mechanically mixed composition (**Figures 4(b)** and **4(c)**) shows remarkably aggregated Ag nanoparticles on the top surface of ZnO indicating improper contact between the composites.

Figure 5 shows the H_2-TPR patterns of AgZn, AuZn and $Ag_{1-y}Au_y/ZnO$ (y = 0.25 and 0.5) catalysts. The TPR pattern of AgZn catalyst showed only a major peak at 192.5ºC and AuZn catalyst showed one main weak TPR peak at 132.4ºC. These peaks indicated the presence of Ag_2O and gold oxide in the AgZn and AuZn catalysts (45, 46). The fact that the XRD analysis of AuZn catalyst did not reveal the presence of any Au oxide species (**Figure 1**), this may suggest that gold oxide crystallites are highly dispersed on the surface and/or Au crystallite sizes are smaller than 5 nm (47). Although AgZn and AuZn have approximately the same

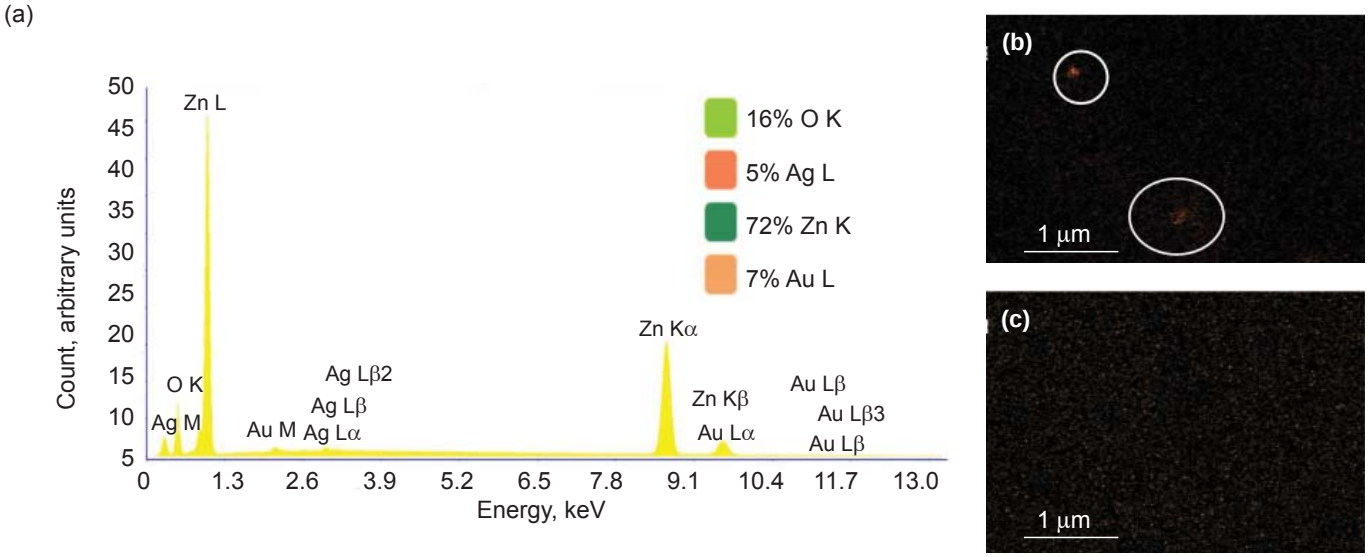

Fig. 4. $(Ag_{0.5}Au_{0.5}Zn)_{mix}$: (a) EDX spectrum; (b) EDX mapping for Ag element: the region of mapping corresponds to (a), acquisition time 665.4 s; (c) EDX mapping for Au element; acquisition time 655.4 s

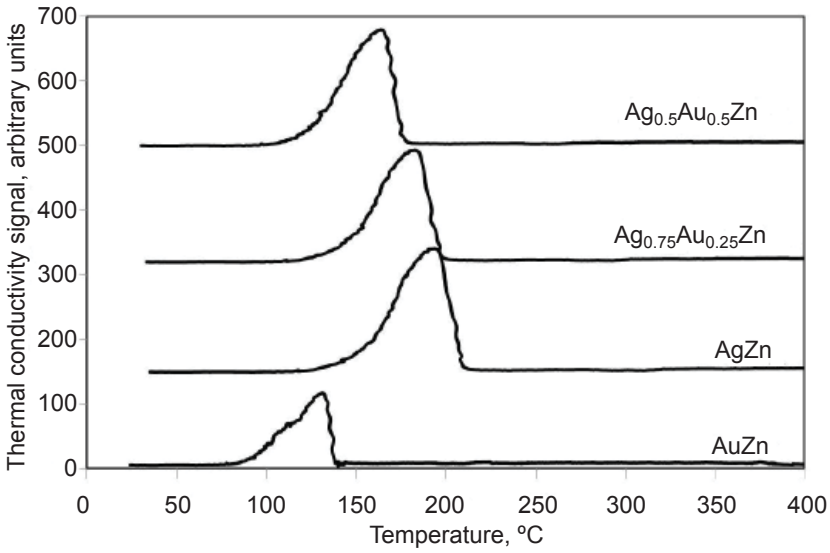

Fig. 5. Temperature-programmed reduction profiles of monometallic AgZn and AuZn catalysts and bimetallic $Ag_{1-y}Au_yZn$ (y = 0.25 and 0.5) catalysts

amount (wt%) of Ag and Au (**Table I**), yet the hydrogen consumption for AuZn was markedly lower than that for AgZn sample (**Figure 5**). This indicates that the majority of Au nanoparticles exist in a metallic state. On the other hand, the TPR features of $Ag_{1-y}Au_y$/ZnO catalysts did not significantly change compared with AgZn. However, adding Au to AgZn catalyst promoted Ag_2O reduction, namely the TPR peak characteristics of Ag_2O reduction was shifted toward a lower temperature. As the Au content increased from 1.25 wt% to 2.5 wt% the main peak shifted from 179.8ºC to 163.2ºC.

The UV/Vis diffuse-reflectance spectra of the monometallic Ag/ZnO and Au/ZnO catalysts as well as three bimetallic catalysts ($Ag_{0.75}Au_{0.25}Zn$, $Ag_{0.5}Au_{0.5}Zn$ and $(Ag_{0.5}Au_{0.5}Zn)_{mix}$) are compared in **Figure 6**. As evident from **Figure 6** curve A for Ag/Zn and curve E for Au/Zn, the obtained spectra of the monometallic catalysts reduced at 300ºC show a broad absorption band due to the surface plasmon resonance (SPR) of Ag and Au nanoparticles at *ca.* 480 nm and 546 nm, respectively (26, 48). In addition, one plasmon band was observed for each bimetallic system and

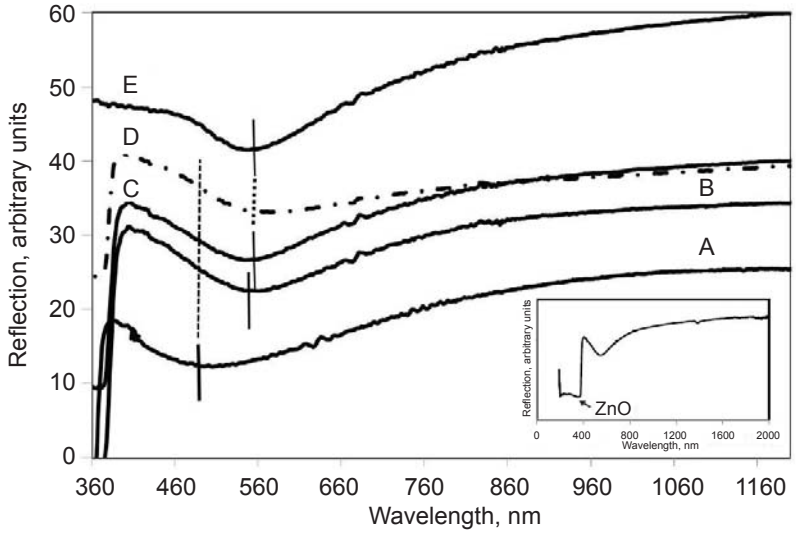

Fig. 6. UV-visible spectra of diffuse reflectance of the monometallic and bimetallic catalysts: **A** Ag/Zn; **B** $Ag_{0.75}Au_{0.25}Zn$; **C** $Ag_{0.5}Au_{0.5}Zn$; **D** $(Ag_{0.5}Au_{0.5}Zn)_{mix}$; **E** Au/ZnO

the plasmon maximum was red-shifted from 480 nm to 540 nm with increasing Au content as shown in **Figure 6** curves B and C, suggesting the formation of Au-Ag alloy (49). However the plasmon band characteristic of $(Ag_{0.5}Au_{0.5}Zn)_{mix}$ (**Figure 6** curve D) was wider than that of $Ag_{0.5}Au_{0.5}Zn$ prepared by DP. It seems that this peak can decompose to two surface plasmon peaks corresponding to the monometallic counterparts. Furthermore, **Figure 6** inset shows a typical band at 400 nm which is characteristic of ZnO (50).

Hydrogen, CO, CO_2 and H_2O production rates at 250ºC and at *ca.* 5% methanol conversion over monometallic and bimetallic $Ag_xAu_{1-x}Zn$ catalysts are presented in **Figure 7**. It is clear that adding Au increased the selectivity of AgZn catalyst towards hydrogen and CO_2. The optimal performance in methanol oxidation to hydrogen was achieved by $Ag_{0.5}Au_{0.5}Zn$ catalyst. However, as shown in **Figure 7**, selectivity toward CO and H_2O decreased with increasing Au content and reached a minimum in the case of $Ag_{0.5}Au_{0.5}Zn$ catalyst. Furthermore, a complementary investigation to confirm synergism between Ag and Au, including theoretical calculations, showed that the experimentally measured rates of hydrogen formation over AgAuZn catalysts are higher than the calculated ones (**Figure 8**). On the other hand, AgZn catalyst showed a decrease in the

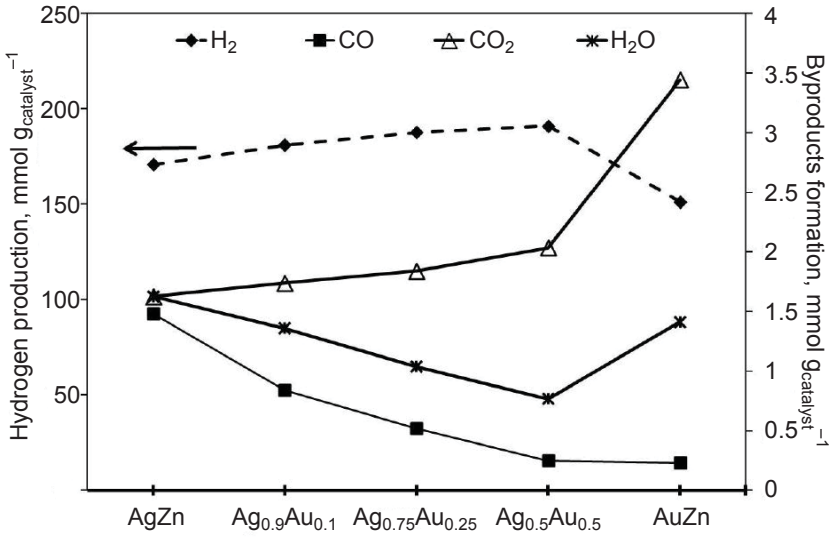

Fig. 7. Hydrogen and byproducts (CO_2, H_2O and CO) production rates over monometallic catalysts and bimetallic $Ag_{1-x}Au_xZn$ catalysts at 250ºC and iso-conversion 5%

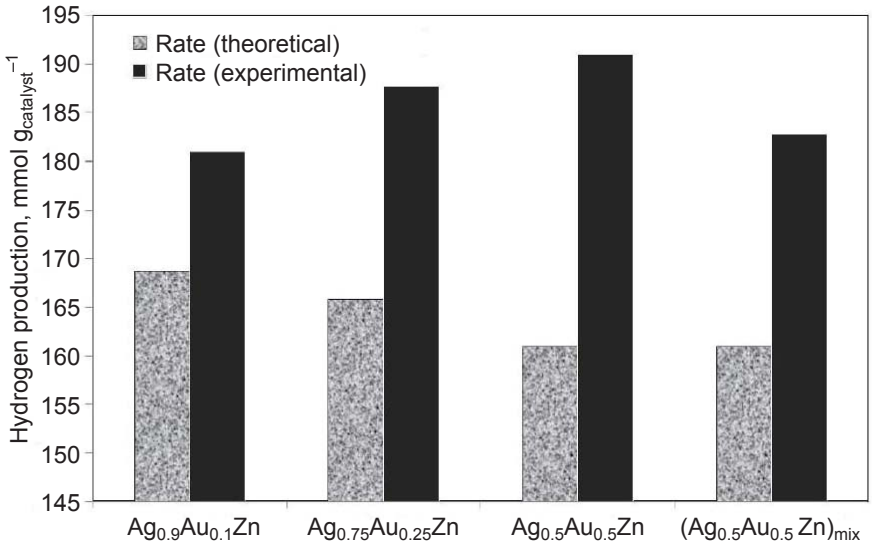

Fig. 8. Comparison between experimental and theoretical rates of hydrogen production over AgAuZn catalysts at 250ºC and iso-conversion 5%

activity during 20 h time-on-stream (TOS) (**Figure 9**). In contrast, a stable activity was observed after *ca.* 7 h TOS for $Ag_{0.5}Au_{0.5}Zn$ catalyst up to 72 h (**Figure 9** inset).

A significant contribution of CO from methanol decomposition and/or reverse water gas shift (Equations (ii) and (iii)) was observed over Ag/ZnO catalyst; however, a decrease in CO formation over bimetallic AgAuZn catalysts was observed. This can be explained by the presence of Au particles, possibly by consuming oxygen with preferential oxidation of CO to CO_2 (Equation (iv)) (26–32). This suggestion runs in good harmony with the observed increase of the rate of CO_2 formation over AgAuZn catalysts especially $Ag_{0.5}Au_{0.5}Zn$ catalyst. Sasirekha *et al.* (28) discussed the effect of promoting Ag catalyst with Au for the preferential oxidation of CO in a hydrogen-rich stream. It could be proposed that the formation of bimetallic alloy in Au-Ag/cerium(IV) oxide (CeO_2) catalyst with Au/Ag ratio of 5:5, which showed a lower reduction temperature, is the reason for its excellent performance toward CO to CO_2 reaction. Herein, the probable interaction between Au and Ag (XRD, TPR, EDX mapping, UV/Vis reflectance and N_2O chemisorptions) may be responsible for improving CO oxidation to CO_2.

$$CH_3OH \rightarrow CO + 2H_2 \quad \text{(ii)}$$

$$CO_2 + H_2 \rightarrow CO + H_2O \quad \text{(iii)}$$

$$CO + O_2 \rightarrow CO_2 \quad \text{(iv)}$$

Adjusting the valency of Ag species could lead to a variation in both hydrogen and CO selectivity. Ag on non-doped AgZn catalyst exists as Ag_2O (as shown by XRD), namely it is in the Ag^+ state. Ag^+ is regarded as an inactive state for POM to hydrogen (24). On the other hand, it was reported that Ag^+ is active in the conversion of methanol to CO. H_2-TPR results showed that adding Au induced a change in the reduction profile of Ag^+ species and may result in the more active species Ag^{n+} (n <1.0) on the AgAuZn catalysts surface. These Ag species may speed up the rate of hydrogen formation and decrease the rate of CO formation. Similarly, Yang *et al.* have reported that the reduction of CuO was enhanced by the presence of Au in Cu/ZnO (6). The enhanced reducibility of CuO has been explained in terms of the tendency of Au to decrease the strength of the Cu–O bond located in the vicinity of Cu. Therefore, it can be suggested that the Ag–O bond was weakened by the presence of Au which seems to be due to a certain degree of interaction between Au and Ag oxides in these catalysts.

In order to test the idea that the reduction of Ag_2O is enhanced by the presence of Au, the $(Ag_{0.5}Au_{0.5}Zn)_{mix}$ catalyst was also synthesised by mechanical mixing to decrease contact between Ag and Au particles. Interestingly, the $(Ag_{0.5}Au_{0.5}Zn)_{mix}$ catalyst showed a lower hydrogen production rate than that of $Ag_{0.5}Au_{0.5}Zn$ catalyst prepared by DP (**Figure 8**). In particular, as shown from the TEM micrograph and EDX mapping of

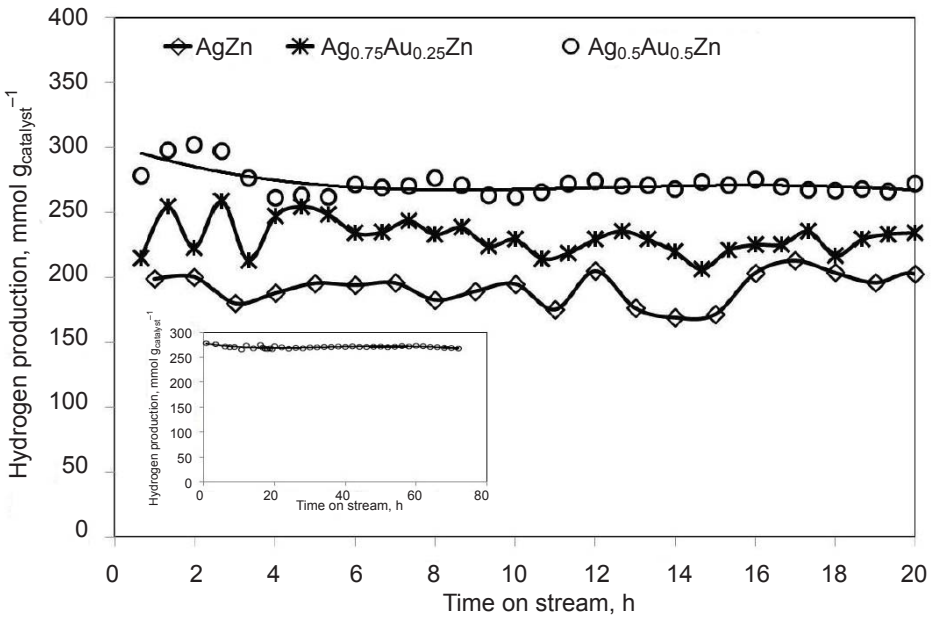

Fig. 9. Time course of the methanol conversion over AgZn catalyst and bimetallic $Ag_{1-y}Au_yZn$ (y = 0.25 and 0.5) catalysts at 350ºC and iso-conversion 5%

the $(Ag_{0.5}Au_{0.5}Zn)_{mix}$, the contact between Ag and Au particles was lower than that between these particles in $Ag_{0.5}Au_{0.5}Zn$ (**Figure 2(c)**). These findings may support the interpretation that the synergetic effects between Ag and Au were due to the strong interaction between Ag and Au nanoparticles (as show by UV-Vis). Furthermore, one cannot exclude that the synergetic effects between interacting Ag and Au in $Ag_{0.5}Au_{0.5}Zn$ catalyst (prepared by DP) for production of hydrogen may also be due to the hydrogen spillover effect (24). Hydrogen adsorbed on Ag sites may be spilt over to neighbouring Au particles in high contact (51), which are known to have high affinity for adsorbing hydrogen (52). The spillover hydrogen on Au particles may be desorbed as hydrogen through ZnO rather than being oxidised to water.

Even though adding Au to AgZn catalyst decreased metal dispersion however, dispersion of metal particles in bimetallic AgAu/ZnO catalysts did not significantly change after reaction compared with AgZn catalyst (**Table I**). This can explain the observed higher stability of bimetallic $Ag_{0.5}Au_{0.5}Zn$ catalyst with 72 h on stream (**Figure 9** inset) during POM reaction at 350ºC.

4. Conclusions

Bimetallic AgAuZn catalyst samples produced a lower amount of CO than AgZn catalyst which encourages the use of these catalysts in a hydrogen fuel cell to avoid any deactivation. The bimetallic catalysts containing 2.5 wt% Ag and 2.5 wt% Au exhibited the highest hydrogen production rate and had the lowest CO production rate. It was suggested that interaction between Ag and Au particles in the AgAuZn catalyst, detected from TPR and UV-Vis results, was responsible for enhancing the reducibility of Ag_2O species in this catalyst. From TEM and EDX mapping investigations it was concluded that the contact between Ag and Au particles in AgAuZn catalyst prepared by DP is greater than that in a comparable catalyst prepared by mechanical mixing. The latter catalyst played an important role in the hydrogen spillover effect. The reaction pathway for POM over AgAuZn involved a preferential oxidation of CO to CO_2 over Au sites.

Acknowledgement

The author would like to thank the supporters of the King Faisal University, Saudi Arabia, and the School of Catalysis at the Egyptian Petroleum Research Institute who generously made resources available to undertake this study.

References

1. L. Mo, X. Zheng and C.-T. Yeh, *ChemPhysChem*, 2005, **6**, (8), 1470
2. C.-T. Yeh, Y.-J. Chen and H.-S. Hung, 'A Process of Producing Hydrogen under Low Temperature', *Taiwan Patent* 226,308; 2005
3. T.-C. Ou, F.-W. Chang and L. S. Roselin, *J. Mol. Catal. A: Chem.*, 2008, **293**, (1–2), 8
4. F.-W. Chang, T.-C. Ou, L. S. Roselin, W.-S. Chen, S.-C. Lai and H.-M. Wu, *J. Mol. Catal. A: Chem.*, 2009, **313**, (1–2), 55
5. V. Dal Santo, A. Gallo, A. Naldoni, M. Guidotti and R. Psaro, *Catal. Today*, 2012, **197**, (1), 190
6. H.-C. Yang, F.-W. Chang and L. S. Roselin, *J. Mol. Catal. A: Chem.*, 2007, **276**, (1–2), 184
7. Y.-C. Lin, K. L. Hohn and S. M. Stagg-Williams, *Appl. Catal. A: Gen.*, 2007, **327**, (2), 164
8. Y.-J. Huang, K. L. Ng and H.-Y. Huang, *Int. J. Hydrogen Energy*, 2011, **36**, (23), 15203
9. E. Qayyum, V. A. Castillo, K. Warrington, M. A. Barakat and J. N. Kuhn, *Catal. Commun.*, 2012, **28**, 128
10. H. Zhu, Z. Guo, X. Zhang, K. Han, Y. Guo, F. Wang, Z. Wang and Y. Wei, *Int. J. Hydrogen Energy*, 2012, **37**, (1), 873
11. C. Pojanavaraphan, A. Luengnaruemitchai and E. Gulari, *Appl. Catal. A: Gen.*, 2013, **456**, 135
12. C. Pojanavaraphan, A. Luengnaruemitchai and E. Gulari, *Int. J. Hydrogen. Energy*, 2013, **38**, (3), 1348
13. S. Pongstabodee, S. Monyanon and A. Luengnaruemitchai, *J. Ind. Eng. Chem.*, 2012, **18**, (4), 1272
14. F.-W. Chang, L. S. Roselin and T.-C. Ou, *Appl. Catal. A: Gen*., 2008, **334**, (1–2), 147
15. M.-L. Xu, X.-K. Yang, Y.-J. Zhang, S.-B. Xia, P. Dong and G.-T. Yang, *Rare Metals*, 2015, **34**, (1), 12
16. R. Feng, M. Li and J. Liu, *Rare Metals*, 2012, **31**, (5), 451
17. I. T. Schwartz, A. P. Jonke, M. Josowicz and J. Janata, *Catal. Lett.*, 2013, **143**, (7), 636
18. M. Rashid, T.-S. Jun, Y. Jung and Y. S. Kim, *Sens. Actuators B: Chem.*, 2015, **208**, 7
19. J. Cao, M. Guo, J. Wu, J. Xu, W. Wang and Z. Chen, *J. Power Sources*, 2015, **277**, (1), 155
20. Y. Tong, J. Pu, H. Wang, S. Wang, C. Liu and Z. Wang, *J. Electroanal. Chem.*, 2014, **728**, 66

21. Y. Luo, Y. Xiao, G. Cai, Y. Zheng and K. Wei, *Fuel*, 2012, **93**, 533
22. S. H. Israni and M. P. Harold, *J. Membrane Sci.*, 2011, **369**, (1–2), 375
23. L. Mo, X. Zheng and C.-T. Yeh, *Chem. Commun.*, 2004, (12), 1426
24. L. Mo, A. H. Wan, X. Zheng and C.-T. Yeh, *Catal. Today*, 2009, **148**, (1–2), 124
25. H. M. AbdelDayem, S. S. Al-Shihry and S. A. Hassan, *Ind. Eng. Chem. Res.*, 2014, **53**, (51), 19884
26. A. Sandoval, A. Aguilar, C. Louis, A. Traverse and R. Zanella, *J. Catal.*, 2011, **281**, (1), 40
27. Z. Qu, G. Ke, Y. Wang, M. Liu, T. Jiang and J. Gao, *Appl. Surf. Sci.*, 2013, **277**, 293
28. N. Sasirekha, P. Sangeetha and Y.-W. Chen, *J. Phys. Chem. C*, 2014, **118**, (28), 15226
29. G. Nagy, T. Benkó, L. Borkó, T. Csay, A. Horváth, K. Frey and A. Beck, *React. Kinet. Mech. Catal.*, 2015, **115**, (1), 45
30. J. H. Byeon and J.-W. Kim, *ACS Appl. Mater. Interfaces*, 2014, **6**, (5), 3105
31. Y. Iizuka, R. Inoue, T. Miura, N. Morita, N. Toshima, T. Honma and H. Oji, *Appl. Catal. A: Gen.*, 2014, **483**, 63
32. T. Déronzier, F. Morfin, M. Lomello and J.-L. Rousset, *J. Catal.*, 2014, **311**, 221
33. W. Li, A. Wang, X. Liu and T. Zhang, *Appl. Catal. A: Gen.*, 2012, **433–434**, 146
34. X. Huang, X. Wang, M. Tan, X. Zou, W. Ding and X. Lu, *Appl. Catal. A: Gen.*, 2013, **467**, 407
35. X. Huang, X. Wang, X. Wang, X. Wang, M. Tan, W. Ding and X. Lu, *J. Catal.*, 2013, **301**, 217
36. L. V. Romashov, L. L. Khemchyan, E. G. Gordeev, I. O. Koshevoy, S. P. Tunik and V. P. Ananikov, *Organometallics*, 2014, **33**, (21), 6003
37. P. M. More, D. L. Nguyen, P. Granger, C. Dujardin, M. K. Dongare and S. B. Umbarkar, *Appl. Catal. B: Environ.*, 2015, **174–175**, 145
38. D. X. Huy, H.-J. Lee, Y. B. Lee and W. S. Choi, *J. Colloid Interface Sci.*, 2014, **425**, 178
39. J. Zheng, H. Lin, Y.-n. Wang, X. Zheng, X. Duan and Y. Yuan, *J. Catal.*, 2013, **297**, 110
40. S. Rojluechai, S. Chavadej, J. W. Schwank and V. Meeyoo, *Catal. Commun.*, 2007, **8**, (1), 57
41. G. C. Bond, C. Louis and D. T. Thompson, "Catalysis by Gold", Catalytic Science Series, Vol. 6, Imperial College Press, London, UK, 2006
42. T. Mallat and A. Baiker, *Ann. Rev. Chem. Biomol. Eng.*, 2012, **3**, 11
43. F. Zane, V. Trevisan, F. Pinna, M. Signoretto and F. Menegazzo, *Appl. Catal. B: Environ.*, 2009, **89**, (1–2), 303
44. J. Zhang, B. Lai, Z. Chen, S. Chu, G. Chu and R. Peng, *Nanoscale Res. Lett.*, 2014, **9**, 237
45. Y. Hu, W. Lü, D. Liu, J. Liu, L. Shi and Q. Sun, *J. Nat. Gas Chem.*, 2009, **18**, (4), 445
46. F. Yinga, S. Wang, C.-T. Au and S.-Y. Lai, *Gold Bull.*, 2010, **43**, (4), 241
47. C.-K. Chang, Y.-J. Chen and C.-t. Yeh, *Appl. Catal. A: Gen.*, 1998, **174**, (1–2), 13
48. A. N. Pestryakov, N. E. Bogdanchikova and A. Knop-Gericke, *Catal. Today*, 2004, **91–92**, 49
49. S. Link and M. A. El-Sayed, *J. Phys. Chem. B*, 1999, **103**, (40), 8410
50. T. Xu, L. Zhang, H. Cheng and Y. Zhu, *Appl. Catal. B: Environ.*, 2011, **101**, (3–4), 382
51. L.-T. Weng and B. Delmon, *Appl. Catal. A: Gen.*, 1992, **81**, (2), 141
52. C. Kartusch and J. A. van Bokhoven, *Gold Bull.*, 2009, **42**, (4), 343

The Author

Hany AbdelDayem holds a BSc degree in Chemistry and an MSc in catalysis from Ain Shams University, Egypt, as well as a PhD in Chemistry for research on chemical kinetics and catalysis from the Université Catholique de Louvain, Belgium. He subsequently held a Fulbright postdoctoral award at the University of Pittsburgh, USA, and a postdoctoral fellowship from the Agence Universitaire de la Francophonie (AUF) at the Université Catholique de Louvain. In 2001 he was appointed Assistant Professor in the Chemistry Department at Ain Shams University. He joined King Faisal University, Saudi Arabia, as Assistant Professor from 2005 up to 2014. In 2015 he is the appointing Associate Professor in physical chemistry at Ain Shams University. His main focus is the development of heterogeneous catalytic processes, including petrochemical and green energy. He is particularly interested in catalyst synthesis, *ex-* and *in situ* characterisation of catalysts and reaction kinetics.

